



ORIGINAL ARTICLE

Cyclometalated complexes containing ferrocenyl Schiff base: Preparation, characterization, DFT calculations, application in cancer and biological researches and MOE studies

Walaa H. Mahmoud^a, Reem G. Deghadi^{a,*}, Gehad G. Mohamed^{a,b}

^a Chemistry Department, Faculty of Science, Cairo University, Giza 12613, Egypt

^b Egypt Nanotechnology Center, Cairo University, 6th October City, El-Sheikh Zayed, Giza 12588, Egypt

Received 19 June 2019; accepted 18 March 2020

Available online 9 April 2020

KEYWORDS

Schiff base;
DFT calculations;
Antimicrobial activities;
Anticancer activities;
Docking

Abstract A series of transition metal (II/III) complexes containing organometallic Schiff base ligand (H₂L) had been synthesized and characterized by using elemental analysis (C, H, N, M), molar conductivity, IR, UV–Vis, ¹H NMR and mass spectral analysis. Also, their TG and DTG behaviors were investigated. The ligand was prepared by condensation of 4-aminosalicylic acid with 2-acetylferrocene in 1:1 M ratio. The data of elemental analysis indicated that the prepared complexes were synthesized also in a 1:1 M ratio. The ligand behaved as neutral bidentate ligand that coordinated to metal ions through protonated *O*-phenolic and protonated carboxylic-OH groups. All complexes had octahedral structure. DFT calculations for H₂L ligand were determined with some parameters such as HOMO-LUMO energy gap, electronegativity and chemical hardness–softness. Antimicrobial activity of both H₂L Schiff base ligand and its metal complexes was tested against different strains of bacteria and fungi species. Furthermore, all compounds had been screened for their anticancer activities against breast cancer (MCF-7) cell line. [Cu(H₂L)(H₂O)₂Cl₂]-2H₂O complex had the lowest IC₅₀ value = 47.3 μg/mL. For determining the more effective and probable binding mode between the H₂L ligand, Co(II) and Zn(II) complexes with different active sites of 4K3V, 2YLB and 3DJD receptors, so molecular docking studies were investigated.

© 2020 The Author(s). Published by Elsevier B.V. on behalf of King Saud University. This is an open access article under the CC BY-NC-ND license (<http://creativecommons.org/licenses/by-nc-nd/4.0/>).

* Corresponding author.

E-mail addresses: reemgd90@yahoo.com, gamalreem56@gmail.com (R.G. Deghadi).

Peer review under responsibility of King Saud University.



Production and hosting by Elsevier

1. Introduction

Organometallic chemistry is a branch of science that deals with chemical compounds which containing at least one bond between a metal and a carbon atom of an organic compound. The prepared organometallic compounds have wide applications in different fields such as: homogeneous catalysis,

stoichiometric processes and medicinal biochemistry (Mudi et al., 2015). Their applications in medicine and biology become very substantial area to be studied. So, broad range of antitumor species has been developed which mainly based on transition-metal arene, cyclopentadienyl and related structures (Brujininx and Sadler, 2008). They have other applications such as in sensors and monitoring protein-protein interactions. Also, they can be used as radioisotopes that may be effective in radioimaging and therapy (Scheck and Schepartz, 2011; Bartholoma et al., 2009; Alberto, 2010) (see Scheme 1).

Ferrocene behaved as one of the most important example of organometallic compounds which discovered in the beginning of 1950s. This led to various advances in organometallic chemistry and other fields (Kealy and Pauson, 1951). It gave good cytotoxicities in vitro and also inhibited the progress of tumors in vivo (Kopf-Maier et al., 1984; Popova et al., 1993). Some researchers showed that addition of ferrocenyl unit to biologically active molecules may lead to formation of complexes with tumor specificity and high potency. The results of increasing the activity may be due to the combined action that occurred of the organic molecule with Fenton chemistry of the Fe center (Hillard, 2006; Auzias, 2009). It also used as a catalyst in industry, contrast agents in magnetic resonance imaging (MRI), antimalaria drugs and anticancer agents in medicine (Salmain et al., 2008; Fouda et al., 2007; Samouei et al., 2011). Nowadays, the scientists try to prepared more derivatives of ferrocene complexes hoping of exploring more materials used in advanced effective applications.

In the light of these facts, and the higher activity of ferrocenyl Schiff base ligand against different bacterial and fungal species, we interested in synthesis of an organometallic Schiff base ligand (H_2L) by condensation of 4-aminosalicylic acid and 2-acetylferrocene was described. Then their Cr(III), Mn(II), Fe(III), Co(II), Ni(II), Cu(II), Zn(II) and Cd(II) complexes were synthesized. All compounds were characterized using different spectroscopic techniques. Also, their antimicrobial and anticancer activities were investigated. DFT calculations were determined and then the data of the experimental IR and UV-Vis results was compared with the theoretical one. Molecular docking was used to predict the probable binding mode between the Schiff base, Co(II) and Zn(II) complexes with the active sites of three receptors which were crystal structure of *Staphylococcus aureus* (PDB ID: 4K3V), crystal structure of *Salmonella typhimurium* (PDB ID: 2YLB) and crystal

structure of deglycating enzyme fructosamine oxidase from *Aspergillus fumigatus* (PDB ID: 3DJD).

2. Experimental

2.1. Materials and reagents

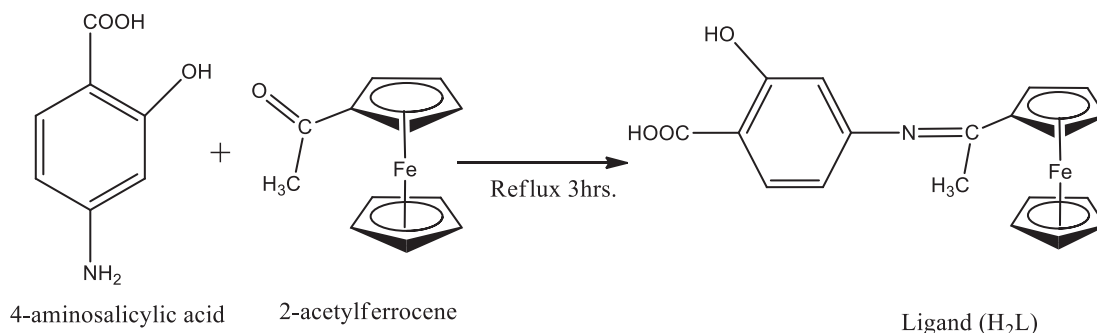
All chemicals used were of the analytical reagent grade (AR) and of highest purity. The chemicals used included 2-acetylferrocene which was supplied from Sigma-Aldrich, 4-aminosalicylic acid (Sigma-Aldrich), $CrCl_3 \cdot 6H_2O$, $MnCl_2 \cdot 2H_2O$ and $FeCl_3 \cdot 6H_2O$ (Sigma-Aldrich), $NiCl_2 \cdot 6H_2O$, $CoCl_2 \cdot 6H_2O$, $CuCl_2 \cdot 2H_2O$ and $ZnCl_2$ (BDH) and $CdCl_2$ (Merck). Organic solvents used were ethyl alcohol (95%), methyl alcohol and *N,N*-dimethylformamide (DMF). Deionized water was usually used in all preparations.

2.2. Solutions

Stock solutions of the ferrocene Schiff base ligand and its metal complexes of $1 \times 10^{-3} \text{ Mol L}^{-1}$ were prepared by dissolving an accurately weighed amount in *N,N*-dimethylformamide for H_2L ligand, Fe(III), Cu(II) and Cd(II) complexes while in 1:1 mixture of DMF:DMSO for Cr(III), Mn(II), Co(II), Ni(II) and Zn(II) complexes. The conductivity then measured for the $1 \times 10^{-3} \text{ Mol L}^{-1}$ solution of metal complexes. Dilute solutions of the Schiff base ligand and its metal complexes ($1 \times 10^{-4} \text{ Mol L}^{-1}$) were prepared by accurate dilution from the previous prepared stock solutions for measuring their UV-Vis spectra.

2.3. Solution of anticancer study

A fresh stock solution ($1 \times 10^{-3} \text{ Mol L}^{-1}$) of Schiff base ligand ($0.12 \times 10^{-2} \text{ g L}^{-1}$) was prepared in the appropriate volume of DMF (90%). DMSO was used in cryopreservation of cells. RPMI-1640 medium was used. The medium was used for culturing and maintenance of the human tumor cell line. The medium was supplied in a powder form. It was prepared as follows: 10.40 g of medium was weighed, mixed with 2 g of sodium bicarbonate, completed to 1 L with distilled water and shaken carefully until complete dissolution. The medium was then sterilized by filtration in a Millipore bacterial filter (0.22 mL). The prepared medium was kept in a refrigerator



Scheme 1 Preparation of organometallic Schiff base ligand (H_2L).

(4 °C) and checked at regular intervals for contamination. Before use, the medium was warmed at 37 °C in a water bath and supplemented with penicillin–streptomycin and FBS. Sodium bicarbonate was used for the preparation of RPMI-1640 medium. Isotonic trypan blue solution (0.05%) was prepared in normal saline and was used for viability counting. FBS (10%, heat inactivated at 56 °C for 30 min), 100 units/mL penicillin and 2 mg/mL streptomycin were used for the supplementation of RPMI-1640 medium prior to use. Trypsin ($0.25 \times 10^{-1}\%$ w/v) was used for the harvesting of cells. Acetic acid (1% v/v) was used for dissolving unbound SRB dye. SRB (0.40%) dissolved in 1% acetic acid was used as a protein dye. A stock solution of trichloroacetic acid (50%) was prepared and stored. An amount of 50 μ L of the stock was added to 200 μ L of RPMI-1640 medium per well to yield a final concentration of 10% used for protein precipitation. Isopropanol (100%) and ethanol (70%) were used. Tris base (10 mM; pH = 10.50) was used for SRB dye solubilization. Tris base (121.10 g) was dissolved in 1000 mL of distilled water and the pH was adjusted using hydrochloric acid (2 Mol L⁻¹).

2.4. Instrumentation

Microanalyses of carbon, hydrogen and nitrogen were carried out at the Microanalytical Center, Cairo University, Egypt, using a CHNS-932 (LECO) Vario elemental analyzer. Analyses of the metals were conducted by dissolving the solid complexes in concentrated HNO₃, and dissolving the residue in deionized water. The metal content was carried out using inductively coupled plasma atomic absorption spectrometry (ICP-AES), Egyptian Petroleum Research Institute. Fourier transform infrared (FT-IR) spectra were recorded with a PerkinElmer 1650 spectrometer (400–4000 cm⁻¹) as KBr pellets. ¹H NMR spectra, as solutions in DMSO-*d*₆, were recorded with a 300 MHz Varian-Oxford Mercury at room temperature using tetra-methylsilane as an internal standard. Mass spectra were recorded using the electron ionization technique at 70 eV with an MS-5988 GS-MS Hewlett-Packard instrument at the Microanalytical Center, National Center for Research, Egypt. UV–Visible spectra were obtained with a Shimadzu UVmini-1240 spectrophotometer. Molar conductivities of 1×10^{-3} Mol L⁻¹ solutions of the solid complexes were measured using a Jenway 4010 conductivity meter. Thermogravimetric (TG) and differential thermogravimetric (DTG) analyses of the solid complexes were carried out from room temperature to 1000 °C using a Shimadzu TG-50H thermal analyzer. Antimicrobial measurements were carried out at the Microanalytical Center, Cairo University, Egypt. Anticancer activity experiments were performed at the National Cancer Institute, Cancer Biology Department, Pharmacology Department, Cairo University. The optical density (OD) of each well was measured spectrophotometrically at 564 nm with an ELIZA microplate reader (Meter tech. R960, USA).

2.5. Synthesis of organometallic Schiff base ligand (H₂L)

The organometallic Schiff base ligand (H₂L) was prepared by refluxing a hot mixture of 4-aminosalicylic acid (0.031 mol, 4.74 g) dissolved in methanol and 2-acetylferrocene (0.031 mol, 7 g) dissolved also in methanol. The resulting mixture was stirred under reflux for about 3 h at 100–150 °C, dur-

ing which a dark brown solid compound was separated. It was filtered, recrystallized, washed with diethylether and dried in vacuum.

(2-(1-((4-carboxy-3-hydroxyphenyl)imino)ethyl)cyclopenta-2,4-dien-1-yl) (cyclopenta-2,4-dien-1-yl)iron (H₂L). Yield 95%; m.p. 247 °C; dark brown solid. Anal. Calc. for C₁₉H₁₇NO₃Fe (%): C, 62.81; H, 4.68; N, 3.86; Fe, 15.43. Found (%): C, 62.32; H, 4.78; N, 3.35; Fe, 15.01. FT-IR (ν, cm⁻¹): hydroxyl (OH) 3406br, carbonyl (C=O) 1733w, azomethine (C=N) 1650sh, ν(COO)_{asy} 1451 m, ν(COO)_{sym} 1371 s. ¹H NMR (300 MHz, DMSO-*d*₆, δ, ppm): 4.22–4.77 (m, 9H, ferrocene ring), 6.00–7.13 (m, 3H, benzene), 10.0 (s, 1H, carboxylic-OH), 8.75 (s, 1H, phenolic-OH), 1.56 (s, 3H, methyl group of ferrocene). UV–Vis (λ_{max}, nm): 271 (π–π* of ferrocene) and 314 (n–π* of COOH, C=N and OH groups).

2.6. Synthesis of metal complexes

Cr(III), Mn(II), Fe(III), Co(II), Ni(II), Cu(II), Zn(II) and Cd(II) complexes were prepared by a reaction of 1:1 M mixture of hot ethanolic solution (60 °C) of the metal chloride (1.10×10^{-3} mol) and the DMF solution of Schiff base ligand (H₂L) (0.4 g, 1.10×10^{-3} mol). The resulting mixture was stirred under reflux for 1 h, whereupon the complexes precipitated. They were collected by filtration and purified by washing several times with diethyl ether. The solid complexes then dried in desiccator over anhydrous calcium chloride.

2.6.1. [Cr(H₂L)(H₂O)₂Cl₂]Cl·5H₂O

Yield 79%; m.p. > 300 °C; dark brown solid. Anal. Calc. for C₁₉H₃₁Cl₃FeCrNO₁₀ (%): C, 35.21; H, 4.79; N, 2.16; Fe, 8.65; Cr, 8.03. Found (%): C, 34.95; H, 4.15; N, 2.09; Fe, 8.33; Cr, 7.89. Λ_m (Ω⁻¹mol⁻¹cm²) = 65; FT-IR (ν, cm⁻¹): hydroxyl (OH) 3404br, carbonyl (C=O) 1780w, azomethine (C=N) 1652sh, ν(COO)_{asy} 1429 s, ν(COO)_{sym} 1367 m, H₂O stretching of coordinated water 847 s and 800w, (M–O) 537w. UV–Vis (λ_{max}, nm): 267 (π–π* of ferrocene) and 323 (n–π* of COOH, C=N and OH groups).

2.6.2. [Mn(H₂L)(H₂O)₃Cl]Cl·5H₂O

Yield 85%; m.p. > 300 °C; dark brown solid. Anal. Calc. for C₁₉H₃₃Cl₂FeMnNO₁₁ (%): C, 36.02; H, 5.21; N, 2.21; Fe, 8.85; Mn, 8.69. Found (%): C, 35.97; H, 5.14; N, 2.07; Fe, 8.33; Mn, 8.54. Λ_m (Ω⁻¹mol⁻¹cm²) = 58; FT-IR (ν, cm⁻¹): hydroxyl (OH) 3391br, carbonyl (C=O) 1770w, azomethine (C=N) 1652sh, ν(COO)_{asy} 1440 s, ν(COO)_{sym} 1384 m, H₂O stretching of coordinated water 900w and 821w, (M–O) 561w. UV–Vis (λ_{max}, nm): 268 (π–π*).

2.6.3. [Fe(H₂L)(H₂O)₂Cl₂]Cl·2H₂O

Yield 94%; m.p. > 300 °C; dark brown solid. Anal. Calc. for C₁₉H₂₅Cl₃Fe₂NO₇ (%): C, 38.16; H, 4.18; N, 2.34; Fe, 18.75. Found (%): C, 37.99; H, 4.06; N, 2.19; Fe, 18.44. Λ_m (Ω⁻¹mol⁻¹cm²) = 61; FT-IR (ν, cm⁻¹): hydroxyl (OH) 3430br, carbonyl (C=O) 1773w, azomethine (C=N) 1648sh, ν(COO)_{asy} 1428 m, ν(COO)_{sym} 1369 m, H₂O stretching of coordinated water 853 s and 810w, (M–O) 541w. UV–Vis (λ_{max}, nm): 265 (π–π* of ferrocene) and 307 (n–π* of COOH, C=N and OH groups).

2.6.4. $[Co(H_2L)(H_2O)_2Cl_2].3H_2O$

Yield 88%; m.p. > 300 °C; dark brown solid. Anal. Calc. for $C_{19}H_{27}Cl_2FeCoNO_8$ (%): C, 39.11; H, 4.63; N, 2.40; Fe, 9.61; Co, 10.12. Found (%): C, 39.01; H, 4.25; N, 2.22; Fe, 9.26; Co, 9.96. Λ_m ($\Omega^{-1}mol^{-1}cm^2$) = 39; FT-IR (ν , cm^{-1}): hydroxyl (OH) 3382br, carbonyl (C=O) disappear, azomethine (C=N) 1651sh, $\nu(COO)_{asy}$ 1435 m, $\nu(COO)_{sym}$ 1382 m, H_2O stretching of coordinated water 824 s and 800w, (M—O) 560w. UV-Vis (λ_{max} , nm): 267 ($\pi-\pi^*$).

2.6.5. $[Ni(H_2L)(H_2O)_3Cl]Cl.2H_2O$

Yield 86%; m.p. > 300 °C; dark brown solid. Anal. Calc. for $C_{19}H_{27}Cl_2FeNiNO_8$ (%): C, 39.11; H, 4.63; N, 2.40; Fe, 9.61; Ni, 10.12. Found (%): C, 39.03; H, 4.46; N, 2.13; Fe, 9.32; Ni, 9.95. Λ_m ($\Omega^{-1}mol^{-1}cm^2$) = 60; FT-IR (ν , cm^{-1}): hydroxyl (OH) 3412br, carbonyl (C=O) 1760w, azomethine (C=N) 1652sh, $\nu(COO)_{asy}$ 1429 m, $\nu(COO)_{sym}$ 1374 m, H_2O stretching of coordinated water 860 s and 800w, (M—O) 535w. UV-Vis (λ_{max} , nm): 267 ($\pi-\pi^*$ of ferrocene) and 326 ($n-\pi^*$ of COOH, C=N and OH groups).

2.6.6. $[Cu(H_2L)(H_2O)_2Cl_2].2H_2O$

Yield 90%; m.p. > 300 °C; grey solid. Anal. Calc. for $C_{19}H_{25}Cl_2FeCuNO_7$ (%): C, 40.04; H, 4.39; N, 2.46; Fe, 9.83; Cu, 11.15. Found (%): C, 39.78; H, 4.21; N, 2.34; Fe, 9.09; Cu, 11.02. Λ_m ($\Omega^{-1}mol^{-1}cm^2$) = 3; FT-IR (ν , cm^{-1}): hydroxyl (OH) 3431br, carbonyl (C=O) disappear, azomethine (C=N) 1651sh, $\nu(COO)_{asy}$ 1430 m, $\nu(COO)_{sym}$ 1310 s, H_2O stretching of coordinated water 920w and 830w, (M—O) 520 s. UV-Vis (λ_{max} , nm): 277 ($\pi-\pi^*$).

2.6.7. $[Zn(H_2L)(H_2O)_2Cl_2].H_2O$

Yield 78%; m.p. > 300 °C; dark brown solid. Anal. Calc. for $C_{19}H_{23}Cl_2FeZnNO_6$ (%): C, 41.23; H, 4.16; N, 2.53; Fe, 10.13; Zn, 11.75. Found (%): C, 41.11; H, 3.99; N, 2.14; Fe, 10.04; Zn, 11.23. Λ_m ($\Omega^{-1}mol^{-1}cm^2$) = 13; FT-IR (ν , cm^{-1}): hydroxyl (OH) 3442br, carbonyl (C=O) disappear, azomethine (C=N) 1648sh, $\nu(COO)_{asy}$ 1436 m, $\nu(COO)_{sym}$ 1380w, H_2O stretching of coordinated water 920w and 850w, (M—O) 550w. UV-Vis (λ_{max} , nm): 269 ($\pi-\pi^*$).

2.6.8. $[Cd(H_2L)(H_2O)_2Cl_2].3H_2O$

Yield 75%; m.p. > 300 °C; dark brown solid. Anal. Calc. for $C_{19}H_{27}Cl_2FeCdNO_8$ (%): C, 35.85; H, 4.25; N, 2.20; Fe, 8.81; Cd, 17.61. Found (%): C, 35.47; H, 4.11; N, 2.10; Fe, 8.64; Cd, 17.42. Λ_m ($\Omega^{-1}mol^{-1}cm^2$) = 6; FT-IR (ν , cm^{-1}): hydroxyl (OH) 3448br, carbonyl (C=O) disappear, azomethine (C=N) 1652sh, $\nu(COO)_{asy}$ 1447 s, $\nu(COO)_{sym}$ 1384s, H_2O stretching of coordinated water 910w and 824s, (M—O) 550w. 1H NMR (300 MHz, DMSO- d_6 , δ , ppm): 4.22–4.77 (m, 9H, ferrocene ring), 6.00–7.95 (m, 3H, benzene), 10.11 (s, 1H, carboxylic-OH), 8.85 (s, 1H, phenolic-OH), 1.25 (s, 3H, methyl group of ferrocene). UV-Vis (λ_{max} , nm): 262 ($\pi-\pi^*$).

2.7. Spectrophotometric studies

The absorption spectra were recorded for 1×10^{-4} Mol L $^{-1}$ solutions of the free organometallic Schiff base ligand and its metal complexes. The spectra were scanned within the wavelength range from 200 to 700 nm.

2.8. Antimicrobial activity

The in vitro antibacterial and antifungal activity tests were performed through the disc diffusion method (Albert, 1979; Govindaraj and Ramanathan, 2014). The bacterial organisms that have been used were [*Bacillus subtilis*, *Staphylococcus aureus*, *Escherichia coli* and *Salmonella typhimurium*] and fungal species included [*Aspergillus fumigatus* and *Candida albicans*]. Stock solution (0.001 mol) was prepared by dissolving the compounds in DMSO. The nutrient agar medium for antibacterial was (0.5% Peptone, 0.1% Beef extract, 0.2% Yeast extract, 0.5% NaCl and 1.5% Agar-Agar) was prepared, cooled to 47 °C and then seeded with tested microorganisms. After solidification 5 mm diameter holes were punched by a sterile corkborer. The investigated compounds, i.e. Schiff base ligand and its metal complexes, were introduced in Petri-dishes (only 0.1 ml) after dissolving in DMSO at 1.0×10^{-3} Mol L $^{-1}$. These culture plates were then incubated at 37 °C for 20 h for bacteria. The activity was determined by measuring the diameter of the inhibition zone (in mm). The plates were kept for incubation at 37 °C for 24 h and then the plates were examined for the formation of zone of inhibition. The diameter of the inhibition zone was measured in millimeters. Antimicrobial activities were performed in triplicate and the average was taken as the final reading (Chandra et al., 2009).

2.9. Anticancer activity

Potential cytotoxicity of all prepared compounds was tested using the method of Skehan and Storeng (Skehan et al., 1990). Cells were plated in 96-multiwell plate (104 cells/well) for 24 h before treatment with the compounds to allow attachment of cell to the wall of the plate. Different concentrations of the compounds under investigation (0, 5, 12.5, 25, 50 and 100 μ g/ml) were added to the cell monolayer and triplicate wells were prepared for each individual dose. The monolayer cells were incubated with the compounds for 48 h at 37 °C and in 5% CO $_2$ atmosphere. After 48 h, cells were fixed, washed and stained with SRB stain. Excess stain was washed with acetic acid and attached stain was recovered with tris-EDTA buffer. The optical density (O.D.) of each well was measured spectrophotometrically at 564 nm with an ELIZA microplate reader and the mean background absorbance was automatically subtracted and mean values of each drug concentration was calculated. The relation between drug concentration and surviving fraction is plotted to get the survival curve of breast tumor cell line for each compound.

Calculation:

The percentage of cell survival was calculated as follows:

Survival fraction = O.D. (treated cells)/O.D. (control cells). The IC $_{50}$ values (the concentrations of the Schiff base ligand (H_2L) or complexes required to produce 50% inhibition of cell growth). This experiment was repeated three times.

2.10. Computational methodology

DFT and molecular modeling theoretical calculations for organometallic Schiff base ligand (H_2L) was carried out on Gaussian03 package (Frisch et al., 2004) at density functional theory (DFT) level of theory. The molecular geometry for the tested ligand was fully optimized using density functional

theory based on B3LYP method along with the LANL2DZ basis set (LakshmiPraba et al., 2015). The optimized structure of the ligand (H_2L) was visualized using Chemcraft version 1.6 package (Mohamed and Abd El-Wahab, 2005), and Gauss-View version 5.0.9 (Dennington et al., 2009). Quantum chemical parameters such as the highest occupied molecular orbital energy (E_{HOMO}), the lowest unoccupied molecular orbital energy (E_{LUMO}) and HOMO–LUMO energy gap (ΔE) for the investigated molecule were calculated.

2.11. Molecular docking

Molecular docking studies were elaborated using MOE 2008 software and it is rigid molecular docking software. These studies are very important for predicting the possible binding modes of the most active compounds against the receptors of crystal structure of *Staphylococcus aureus* (PDB ID: 4K3V), crystal structure of *Salmonella typhimurium* (PDB ID: 2YLB) and crystal structure of deglycating enzyme fructosamine oxidase from *Aspergillus fumigatus* (PDB ID: 3DJD) (Dhanaraj et al., 2016). Docking is an interactive molecular graphics program can be used to calculate and display feasible docking modes of a receptor and ligand and complex molecules. It necessitates the ligand, the receptor as input in PDB format. The water molecules, co-crystallized ligands and other unsupported elements (e.g., Na, K, Hg, etc.) were removed but the amino acid chain was kept (Balakrishnan et al., 2015). The structure of ligand in PDB file format was created by Gaussian03 software. The crystal structures of the three receptors were downloaded from the protein data bank (<http://www.rcsb.org/pdb>).

3. Results and discussion

3.1. Characterization of organometallic Schiff base ligand (H_2L)

A dark brown organometallic Schiff base ligand (H_2L) was synthesized by condensation between 4-aminosalicylic acid with 2-acetylferrocene. The structure of the prepared ligand was characterized according to different techniques such as elemental analysis, IR, mass spectrometry, 1H NMR UV–Vis and thermal analyses. The mass spectrum (MS) of H_2L ligand showed a peak at 364 amu which corresponding to the molecular ion (m/z) peak. The data confirmed the successful condensation between the parent compounds to get the Schiff base ligand that has molecular formula $C_{19}H_{17}NO_3Fe$ with atomic mass 363 g/mol. The elemental analysis data indicated that the ligand was formed in 1:1 M ratio. The infrared spectrum of the Schiff base ligand showed important characteristic bands. The most characteristic band was appeared at 1650 cm^{-1} that may be corresponded to $\nu(C=N)$ of azomethine group. This gave good indication for the successful synthesis of organometallic Schiff base ligand (Firouzabadi and Firouzmandi, 2017). The stretching frequency of $\nu(OH)$ group was observed at 3406 cm^{-1} as a broad band (Martins et al., 2017). The ligand also exhibited bands at 1733, 1451 and 1371 cm^{-1} due to $\nu(C=O)$, $\nu(COO^-)_{asy}$ and $\nu(COO^-)_{sym}$, respectively (Ajlouni et al., 2016; Mahmoud et al., 2017a). 1H NMR spectrum of H_2L ligand showed multiplet signals that were appeared in

the region of 4.22–4.77 ppm which correspond to the ferrocene protons (Zhang et al., 2001). The signal which was attributed to the methyl protons was observed at 1.56 ppm (Yadav and Singh, 2011). The multi-signals within the 6.00–7.13 ppm range were assigned to the aromatic protons of benzene ring (Bal et al., 2014). In the down field region of the 1H NMR spectrum of the ligand, singlet signal was observed at 10 ppm which related to carboxylic proton of salicylic acid (Bal et al., 2014; Roman and Andree, 2001). Singlet signal was appeared at 8.75 ppm that related to the phenolic proton (Alaghaz et al., 2014a).

3.1.1. Geometrical optimization of the Schiff base ligand (H_2L)

Calculating theoretical parameters would help in characterizing the molecular structure of the prepared compounds. So, the structure of the Schiff base ligand was optimized by using DFT method (Gaber et al., 2018; Singh et al., 2012). The calculated bond lengths and bond angles for H_2L ligand were listed in Supplementary Table (1) and the optimized structure of the H_2L ligand was shown in Fig. 1. Furthermore, other quantum chemical parameters such as: energy of the highest occupied molecular orbital, E_{HOMO} , energy of the lowest unoccupied molecular orbital, E_{LUMO} , energy gap (ΔE), chemical potentials, μ , electronegativity, χ , dipole moment, μ , softness, σ , hardness, η , and additional electronic charge, ΔN_{max} had been calculated according to different equations as shown in Supplementary Information 1 (SI-1) and then were listed in Table 2 (Pearson, 1989; Geerlings et al., 2003; Chattaraj and Giri, 2007).

When the value of E_{HOMO} become higher, the molecule is better for donating electrons. This means that the ligand offering electrons to unoccupied d-orbital of the transition metal ions and this increase the possibility of complexation to occur. Also, the small band gap energy showed that the molecule became more reactive one. The ΔE value of the H_2L ligand was very small (3.98 e.V). Dipole moment is considered as very important role in increasing the biological activities of the prepared compounds. The decrease in this value as observed in the prepared ligand may be the reason for increasing of its activities against breast cancer (Sagdinc et al., 2009).

3.1.2. Molecular electrostatic potential map (MEP)

MEP of the synthesized ligand was observed in Fig. 2. The MEP gave important information about charge density distributions, electrophilic interactions and chemically reactive sites that present in the ligand (Sahin et al., 2017). The positive electrostatic potential surfaces were represented by blue color which referred to the lower electron density regions. The negative regions were represented by red color which corresponded to nucleophilic sites (Ekmekcioglu et al., 2015; Aktan et al., 2011). The MEP of the ligand showed red color which surrounded the carboxylic and phenolic groups. While the ferrocene and benzene rings were surrounded by blue-green color. This indicated that the more reactive sites which were electrophilic surfaces that coordinated to metal ions were phenolic and carboxylic groups (Babur et al., 2015).

3.1.3. Vibrational properties

For confirming the successfully preparation of the ligand, experimentally vibrational analysis was compared with the theoretical data that had been performed based on the optimized

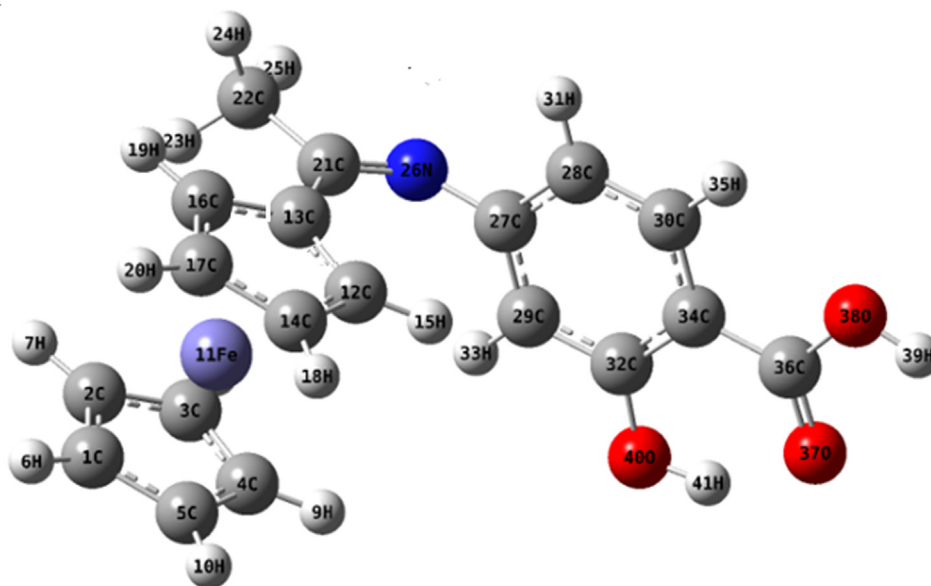


Fig. 1 The optimized structure of organometallic Schiff base ligand (H_2L).

Table 2 The different quantum chemical parameters of organometallic Schiff base ligand (H_2L).

The calculated quantum chemical parameters	
E (a.u)	-1137.97
Dipole moment (Debye)	4.83
E_{HOMO} (eV)	-5.91
E_{LUMO} (eV)	-1.93
ΔE (eV)	3.98
χ (eV)	3.92
η (eV)	1.99
σ (eV) ⁻¹	0.51
π (eV)	-3.92
S (eV) ⁻¹	0.25
ω (eV)	3.86
ΔN_{max}	1.97

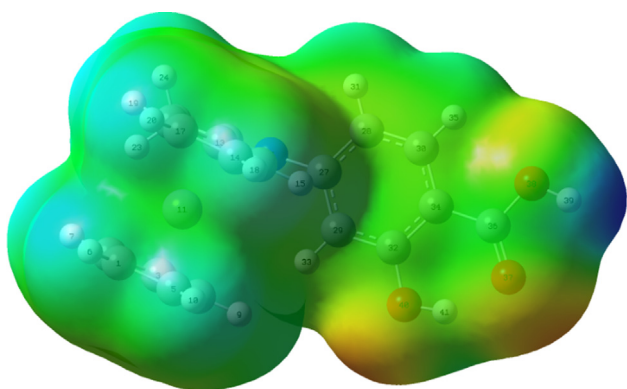


Fig. 2 Molecular electrostatic potential map of organometallic Schiff base ligand (H_2L), the electron density isosurface is 0.004 a.u.

structure of the ligand. The data observed with the quantum chemical methods such as DFT method had systematic errors. So, using scaling factor of 0.96 for LanL2DZ level can overcome these errors (Alturk et al., 2016). The experimental data showed that the ligand had five important characteristic bands which were appeared at 3406, 1733, 1650, 1451 and 1371 cm^{-1} which corresponded to $\nu(OH)$, $\nu(C=O)$, $\nu(C=N)_{azomethine}$, $\nu(COO^-)_{asy}$ and $\nu(COO^-)_{sym}$, respectively. These bands were calculated theoretically and their value were at 3666, 1720, 1680, 1482 and 1389 cm^{-1} . These data confirmed that the experimental values were close to the theoretical data. So, the ligand was prepared with successful method (Mahmoud et al., 2017b; Ermis, 2018).

3.1.4. UV-Visible analysis

The nature of the electronic transitions presented in the UV-Vis spectrum of the Schiff base ligand had been studied by high accuracy and low computational cost of DFT method (Mahmoud et al., 2017c; Reed et al., 1988). The experimental and theoretical electronic spectra of the ligand were showed in Supplementary Fig. 3. Also, electronic transitions with maximum oscillator strength from DFT calculations were listed in Supplementary Table 3. The experimental absorption spectrum of the Schiff base ligand was recorded in 10^{-4} M DMF solution. This spectrum showed bands at 271 and 314 nm which related to $\pi-\pi^*$ transitions of the ferrocene and benzene rings and to the $n-\pi^*$ transition of COOH, OH and C=N groups, respectively (Kucuk et al., 2015).

The data from TD-DFT method showed also two electronic transitions at 277 and 312 nm. The band observed at 277 nm was contributed to transition from HOMO-4 to LUMO. The second band computed at 312 nm with an oscillator strength of $f = 0.3211$ was represented by the contribution of HOMO \rightarrow LUMO + 3 or contribution of HOMO-2 \rightarrow LUMO (Gokce et al., 2017; Bilge et al., 2009). These transitions were shown in Fig. 4.

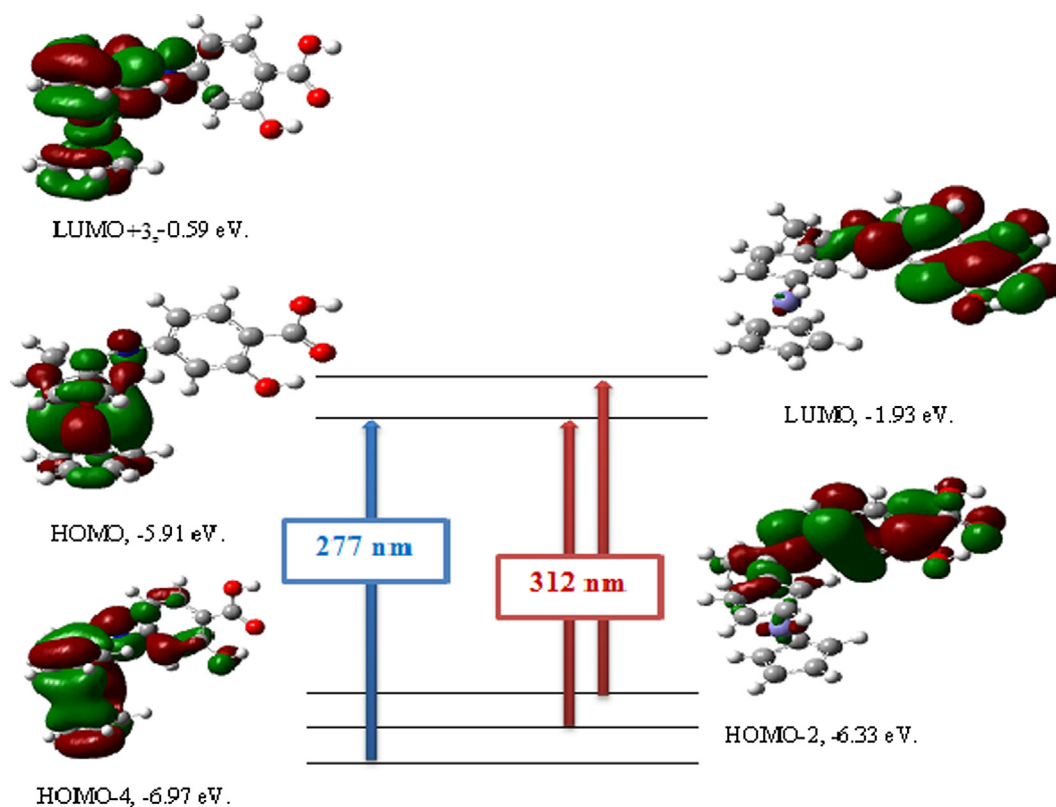


Fig. 4 Theoretical electronic absorption transitions for Schiff base ligand (H_2L) in DMF solvent.

3.2. Characterization of metal complexes

After preparation of organometallic Schiff base ligand, their Cr(III), Mn(II), Fe(III), Co(II), Ni(II), Cu(II), Zn(II) and Cd(II) complexes were also prepared. All the prepared compounds were characterized by using various techniques such as elemental analysis (C, H, N and metal content), IR, molar conductance, UV-Vis, 1H NMR and mass spectrometry. Their thermal analyses (TG and DTG) were studied.

3.2.1. Elemental analysis

The transition metal complexes were also prepared and then collected in pure form with satisfied yields. Their melting points, colors and percent of carbon, hydrogen, nitrogen and metal contents were determined. The complexes agreed well with a 1:1 metal: ligand stoichiometric ratio. They were air stable solids at room temperature and had high melting point values > 300 °C. They were soluble in *N,N*-dimethylformamide (DMF) for H_2L ligand, Fe(III), Cu(II) and Cd(II) complexes while in 1:1 mixture of DMF:DMSO for Cr(III), Mn(II), Co(II), Ni(II) and Zn(II) complexes. Also, they were insoluble in water, ethanol and methanol solutions.

3.2.2. Molar conductivity measurements

The molar conductivity of 10^{-3} Mol L^{-1} solutions of all prepared complexes was measured at room temperature (25 °C). It was shown that Co(II), Cu(II), Zn(II) and Cd(II) complexes were located as non-electrolytes (Gull and Hashmi, 2015; Alothman et al., 2019). The data of these results assigned to the absence of any chloride anion in outer sphere of these com-

plexes. While, Cr(III), Mn(II), Fe(III) and Ni(II) complexes behaved as electrolytes as the result of the presence of chloride anions in the outer sphere (Soliman and Mohamed, 2013; Mohamed et al., 2006).

3.2.3. IR spectra

In order to determine the mode of binding between the Schiff base and metal ions, IR spectra of all prepared complexes were compared with that of the Schiff base ligand. The IR spectrum of H_2L ligand showed band at 1650 cm^{-1} , this band attributed to azomethine group. In all metal complexes spectra, there were not any significant shifting in this band which confirming the non-participating of this azomethine group in the coordination (Firouzabadi and Firouzmandi, 2017). A broad band was appeared in the ligand spectrum at 3406 cm^{-1} . This band was shifted in all complexes to lower or higher frequencies in the range of $3382\text{--}3448\text{ cm}^{-1}$ which confirming the participation of OH group in coordination with metal ions (Martins et al., 2017; Soliman and Mohamed, 2013). The carbonyl group, asymmetric and symmetric vibrations of carboxylic bands were exhibited in ligand at 1733 , 1451 and 1371 cm^{-1} , respectively. These bands were shifted in all metal complexes to $1760\text{--}1780$, $1428\text{--}1447$ and $1310\text{--}1384\text{ cm}^{-1}$, respectively (Ajrouni et al., 2016; Mahmoud et al., 2017d). The shift occurred in the carboxylate bands confirmed its participation in chelate formation with monodentate mode. Furthermore, two bands were assigned to the presence of coordinated water molecules in all metal complexes which appeared at $824\text{--}920$ and $800\text{--}850\text{ cm}^{-1}$ (Mahmoud et al., 2016). In lower frequencies of all metal complexes spectra, new band was found in the

region of 520–561 cm^{-1} which attributed to $\nu(\text{M}-\text{O})$ (Halli et al., 2011). From the comparison between the spectrum of Schiff base and its metal complexes spectra, it was concluded that H_2L ligand behaved as bidentate ligand that can be coordinated to the metal ions through protonated phenolic-OH and protonated carboxylic-OH groups.

3.2.4. ^1H NMR spectra

The ^1H NMR spectra of H_2L ligand and its Cd(II) complex were recorded in $\text{DMSO}-d_6$ (Singh et al., 2010). The spectrum of the ligand showed multiplet signals that appeared in the region of 4.22–4.77 ppm which corresponded to the ferrocene protons (Zhang et al., 2001). These signals were appeared in Cd(II) complex at the same range. The methyl protons was observed as singlet signal at 1.56 ppm in the ligand and at 1.25 ppm in its Cd(II) complex (Yadav and Singh, 2011). The multi-signals within the 6.00–7.13 ppm range were assigned to the aromatic protons of benzene ring in the ligand which were indicated in the Cd(II) complex at 6.00–7.95 ppm (Bal et al., 2014). The carboxylic proton of salicylic acid was observed at 10 ppm in Schiff base ligand. This signal was still appeared in the Cd(II) complex but shifted to higher value at 10.11 ppm. This data indicated that this proton didn't remove from the carboxylic group upon coordination (Bal et al., 2014; Roman and Andree, 2001). Also in the ^1H NMR spectrum of ligand, singlet signal was appeared at 8.75 ppm that related to the phenolic proton (Alaghaz et al., 2014b). This signal was still present in the spectrum of the Cd(II) complex but shifted to higher value 8.85 ppm. This confirmed the participating of this phenolic proton in coordination. Finally, the ligand behaved as neutral bidentate ligand as confirmed from the IR spectra (Fig. 5).

3.2.5. UV-Visible spectra of the Schiff base ligand and its metal complexes

The electronic absorption spectra of the prepared organometallic Schiff base and its metal complexes were measured in the range of 200–700 nm at room temperature.

The absorption spectrum of organometallic Schiff base ligand showed two bands at 271 and 314 nm. The first band was related to $\pi-\pi^*$ transitions of the benzene and ferrocene rings. The second band was observed at $\lambda_{\text{max}} = 314$ nm that may be related to the $n-\pi^*$ transition of the COOH, OH and C=N groups (Soliman and Mohamed, 2013; Kianfar et al., 2013). In all metal complexes, the band that appeared at 271 nm in the ligand was shifted to the range of 262–277 nm. While the other band that related to $n-\pi^*$ transition was shifted to 307–326 nm. These shifting gave good indication for coordination of carboxylic group to the metal ions (Liu et al., 2007; Mahalakshmi and Rajavel, 2010).

3.2.6. Thermal analysis of Schiff base ligand and its metal complexes

Thermal analysis is considered as a very useful, effective and important technique that can be used to determine the thermal stability of materials and confirm their molecular structures. So, the thermal stability of organometallic Schiff base (H_2L) and its transition metal complexes were investigated using differential thermogravimetric (DTG) and thermogravimetric technique (TG) analyses. These analyses were investigated at heating rate of 10 $^\circ\text{C}/\text{min}$ in nitrogen atmosphere over the range from room temperature to 1000 $^\circ\text{C}$. The data then were listed in Table 4.

The organometallic Schiff base ligand (H_2L) with the molecular formula ($\text{C}_{19}\text{H}_{17}\text{NO}_3\text{Fe}$) was thermally decomposed in five decomposition steps. The first and second steps with estimated mass loss of 19.74% (calculated mass loss = 19.84%) within the temperature range 70–405 $^\circ\text{C}$ may be correspond to the loss of $\text{C}_3\text{H}_6\text{NO}$ molecule. The DTG curve gave maximum peaks temperature at 201 and 376 $^\circ\text{C}$. The other three decomposition steps with estimated mass loss of 43.33% (calculated mass loss = 43.80%) within the temperature range 405–1000 $^\circ\text{C}$ may be correspond to the loss of $\text{C}_{11}\text{H}_{11}\text{O}$ molecule. The DTG curve gave maximum peaks temperature at 424, 617 and 735 $^\circ\text{C}$. At the end of decomposition FeO contaminated with carbon remained as residues. The overall weight loss amounted to 63.07% (calculated mass loss = 63.64%).

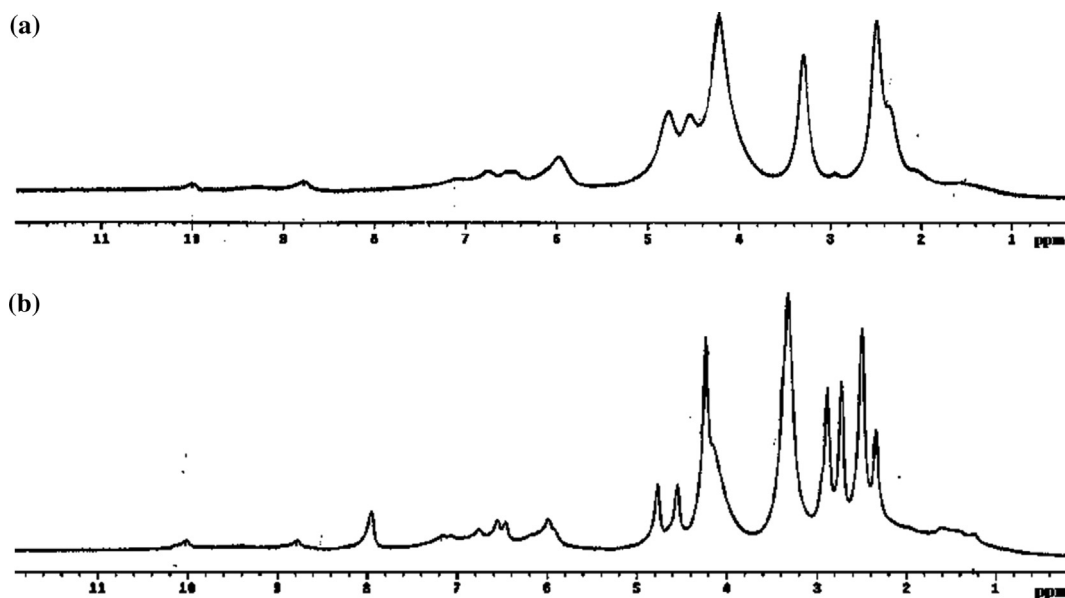


Fig. 5 a ^1H NMR spectrum of Schiff base ligand (H_2L). b ^1H NMR spectrum of $[\text{Cd}(\text{H}_2\text{L})(\text{H}_2\text{O})_2\text{Cl}_2] \cdot 3\text{H}_2\text{O}$ complex.

Table 4 Thermoanalytical results (TG and DTG) of organometallic Schiff base (H₂L) and its metal complexes.

Complex	TG range (°C)	DTG _{max} (°C)	n*	Mass loss (Calc.) %	Total mass lossEstim	Assignment	Residues
Schiff base ligand (H ₂ L)	70–405	201, 376	2	19.74 (19.84)		-Loss of C ₃ H ₆ NO.	
	405–1000	424, 617, 735	3	43.33 (43.80)	63.07 (63.64)	-Loss of C ₁₁ H ₁₁ O	FeO + 5C
[Cr(H ₂ L)(H ₂ O) ₂ Cl ₂]Cl·5H ₂ O	40–125	78	1	13.22 (13.90)		-Loss of 5H ₂ O.	
	125–455	341	1	20.83 (20.54)		-Loss of Cl ₂ , 2H ₂ O and C ₂ H ₂ .	FeO + ¹ / ₂ Cr ₂ O ₃ 4C
	455–1000	847	1	35.72 (35.29)	69.77 (69.73)	-Loss of C ₁₃ H ₁₅ NO _{0.5} Cl.	
[Mn(H ₂ L)(H ₂ O) ₃ Cl]Cl·5H ₂ O	40–145	77	1	13.73 (14.22)		-Loss of 5H ₂ O.	
	145–520	310	1	20.18 (19.75)		-Loss of 3H ₂ O and Cl ₂ .	
	520–1000	660	1	33.92 (33.97)	67.83 (67.94)	-Loss of C ₁₄ H ₁₇ NO.	FeO + MnO + 5C
[Fe(H ₂ L)(H ₂ O) ₂ Cl ₂]Cl·2H ₂ O	30–105	69	1	6.13 (6.03)		-Loss of 2H ₂ O.	
	105–380	144	1	22.96 (22.26)		-Loss of Cl ₂ , 2H ₂ O and C ₂ H ₂ .	FeO + ¹ / ₂ Fe ₂ O ₃ + 5C
	380–1000	616, 925	2	35.16 (36.23)	64.25 (64.52)	-Loss of C ₁₂ H ₁₅ NO _{0.5} Cl.	
[Co(H ₂ L)(H ₂ O) ₂ Cl ₂]·3H ₂ O	30–390	75, 340	2	27.02 (26.85)		-Loss of 5H ₂ O, HCl and C ₂ H ₆ .	
	390–610	590	1	9.72 (9.61)		-Loss of C ₃ H ₄ O.	FeO + CoO + 4C
	610–1000	727	1	30.15 (30.10)	66.89 (66.56)	-Loss of C ₁₀ H ₆ NCl.	
[Ni(H ₂ L)(H ₂ O) ₃ Cl]Cl·2H ₂ O	40–520	89, 340	2	33.23 (33.37)		-Loss of 5H ₂ O, HCl and C ₄ H ₄ O.	FeO + NiO + 4C
	520–1000	843	1	33.22 (33.19)	66.45 (66.56)	-Loss of C ₁₁ H ₁₂ NCl.	
[Cu(H ₂ L)(H ₂ O) ₂ Cl ₂]·2H ₂ O	30–130	85	1	6.43 (6.32)		-Loss of 2H ₂ O.	
	130–345	313	1	18.90 (18.79)		-Loss of 2H ₂ O and Cl ₂ .	
	345–1000	600	1	39.97 (39.86)	65.30 (64.97)	-Loss of C ₁₅ H ₁₇ NO.	FeO + CuO + 4C
[Zn(H ₂ L)(H ₂ O) ₂ Cl ₂]·H ₂ O	40–635	83, 281	2	39.97 (39.60)		-Loss of 3H ₂ O, Cl ₂ and C ₆ H ₆ O.	FeO + ZnO + 5C
	635–1000	580	1	21.67 (21.88)	61.64 (61.48)	-Loss of C ₈ H ₁₁ N.	
[Cd(H ₂ L)(H ₂ O) ₂ Cl ₂]·3H ₂ O	30–325	86, 220	2	13.96 (14.15)		-Loss of 5H ₂ O.	
	325–615	432, 588	2	16.82 (16.75)		-Loss of HCl and C ₃ H ₄ NO.	CdO + FeO
	615–1000	699	1	37.61 (37.66)	68.39 (68.56)	-Loss of C ₁₆ H ₁₂ Cl.	

n* = number of decomposition steps.

The [Cr(H₂L)(H₂O)₂Cl₂]Cl·5H₂O complex was thermally decomposed in three steps. The first step with estimated mass loss of 13.22% (calculated mass loss = 13.90%) within the temperature range of 40–125 °C corresponded to loss of five water molecules of hydration. The DTG curve gave maximum peak temperature at 78 °C. The second step corresponded to estimated mass loss of 20.83% (calculated mass loss = 20.54%) within the temperature range 125–455 °C and represented the loss of Cl₂ gas, 2H₂O and C₂H₂ molecules. The final step with estimated mass loss of 35.72% (calculated mass loss = 35.29%) within the temperature range 455–1000 °C corresponded to loss of C₁₃H₁₅NO_{0.5}Cl molecule. The DTG curve gave maximum peak temperature at 847 °C, leaving FeO and \emptyset Cr₂O₃ contaminated with carbon as residues. The overall weight loss amounted to 69.77% (calculated mass loss = 69.73%).

The [Mn(H₂L)(H₂O)₃Cl]Cl·5H₂O complex upon heating lost 5H₂O molecules in the first step of decomposition within the temperature range 40–145 °C at maximum peak temperature 77 °C, with a mass loss = 13.73% (calculated mass loss = 14.22%). The second step of decomposition occurred at maximum peak temperature at 310 °C, correspond to loss of Cl₂ gas and 3H₂O molecules with a mass loss = 20.18% (calculated mass loss = 19.75%), in the temperature range of 145–520 °C. The final step started the decomposition at 520 °C and ended at 1000 °C with maximum peak temperature

at 660 °C and may be correspond to the loss of C₁₄H₁₇NO molecule with mass loss of 33.92% (calculated mass loss = 33.97%), leaving FeO and MnO oxides contaminated with carbon as residues of decomposition. The overall weight loss amounted to 67.83% (calculated mass loss = 67.94%).

The [Fe(H₂L)(H₂O)₂Cl₂]Cl·2H₂O complex showed four decomposition steps within the range 30–1000 °C. The first decomposition step was accompanied by loss of 2H₂O molecules of hydration in the temperature range of 30–105 °C with an estimated mass loss of 6.13% (calculated mass loss = 6.03%). The DTG curve gave maximum peak temperature at 69 °C (the maximum peak temperature). The second step of decomposition correspond to loss of C₂H₂, 2H₂O molecules and Cl₂ gas at 105–380 °C with an estimated mass loss of 22.96% (calculated mass loss = 22.26%) with maximum peak temperature at 144 °C. The final two decomposition steps within the range 380–1000 °C were assigned to loss of C₁₂H₁₅NO_{0.5}Cl molecule with a mass loss of 35.16% (calculated mass loss = 36.23%). Ferric and ferrous oxides contaminated with carbon were remained as residues. The overall weight loss amounted to 64.25% (calculated mass loss = 64.52%).

In the thermograph of [Co(H₂L)(H₂O)₂Cl₂]·3H₂O complex, the first and second steps of decomposition correspond to mass loss of 27.02% (calculated mass loss = 26.85%) within the temperature range of 30–390 °C with maximum peaks temper-

ature at 75 and 340 °C, represented the loss of 5H₂O, HCl and C₂H₆ molecules. The third step started the decomposition at 390 °C and ended at 610 °C with maximum peak temperature at 590 °C and may be accounted to the loss of C₃H₄O molecule with mass loss of 9.72% (calculated mass loss = 9.61%). The final step of the decomposition started at 610 °C and ended at 1000 °C with maximum peak temperature at 727 °C and may be accounted to the loss of C₁₀H₆NCl molecule with mass loss of 30.15% (calculated mass loss = 30.10%), leaving behind FeO and CoO oxides contaminated with carbon as residues of decomposition. The overall weight loss amounted to 66.89% (calculated mass loss = 66.56%).

In the thermograph of [Ni(H₂L)(H₂O)₃Cl]Cl·2H₂O complex, the first and second steps of decomposition displayed a gradual mass loss of 33.23% (calculated mass loss = 33.37%) within the temperature range of 40–520 °C which may be correspond to the loss of five molecules of water of hydration, HCl and C₄H₄O molecules. The DTG curve gave maximum peaks temperature at 89 and 340 °C. The final step represented a mass loss of 33.22% (calculated mass loss = 33.19%) which correspond to loss of C₁₁H₁₂NCl molecule within temperature range 520–1000 °C. The maximum peak temperature was at 843 °C. Finally, FeO and NiO contaminated with carbon remained as residues. The overall weight loss amounted to 66.45% (calculated mass loss = 66.56%).

The [Cu(H₂L)(H₂O)₂Cl₂].2H₂O complex gave decomposition pattern that started from 30 °C to 1000 °C with three steps. The first step within the temperature range of 30–130 °C with maximum peak temperature at 85 °C which represented the loss of two water molecules of hydration with a found mass loss of 6.43% (calculated mass loss = 6.32%). The second step which represented the loss of Cl₂ gas and 2H₂O molecules with a mass loss of 18.90% (calculated mass loss = 18.79%) within the temperature range 130–345 °C and maximum peak temperature at 313 °C. The final step was represented the loss of C₁₅H₁₇NO molecule with a mass loss of 39.97% (calculated mass loss = 39.86%) within the temperature range 345–1000 °C and maximum peak temperature at 600 °C. At the end of the thermogram, FeO and CuO contaminated with carbon remained as residues. The overall weight loss amounted to 65.30% (calculated mass loss = 64.97%).

In the thermograph of [Zn(H₂L)(H₂O)₂Cl₂].H₂O complex, the first and second decomposition steps displayed a gradual mass loss of 39.97% (calculated mass loss = 39.60%) within the temperature range of 40–635 °C which may be correspond to the loss of three molecules of water, Cl₂ gas and C₆H₆O molecule. The DTG curve gave peaks at 83 and 281 °C (the maximum peaks temperature). The third decomposition step indicated a mass loss of 21.67% (calculated mass loss = 21.88%) which correspond to loss of C₈H₁₁N molecule within temperature range 635–1000 °C. The maximum peak temperature was at 580 °C. Finally FeO + ZnO contaminated with carbon remained as residues. The overall weight loss amounted to 61.64% (calculated mass loss = 61.48%).

The [Cd(H₂L)(H₂O)₂Cl₂].3H₂O complex lost upon heating 5H₂O molecules in the first and second steps of decomposition within the temperature range of 30–325 °C, at maximum peaks temperature at 86 and 220 °C with estimated mass loss of 13.96% (calculated mass loss = 14.15%). The third and fourth

steps accounted for the loss of HCl and C₃H₄NO molecules within the temperature range of 325–615 °C, at maximum peaks temperature at 432 and 588 °C, with estimated mass loss of 16.82% (calculated mass loss = 16.75%). The final step correspond to loss of C₁₆H₁₂Cl molecule within temperature range 615–1000 °C at maximum peak temperature at 699 °C, with estimated mass loss of 37.61% (calculated mass loss = 37.66%), leaving FeO and CdO as residues of decomposition. The overall weight loss amounted to 68.39% (calculated mass loss = 68.56%).

The prepared ferrocenyl ligand had iron atom. During the synthesis of its complexes with different transition metal ions, they contain two metal atoms. Due to that, these prepared complexes were very stable and their M.P. > 300 °C. So, the residues were a mixture of ferrous oxide and transition metal oxide which became contaminated with some carbon atoms.

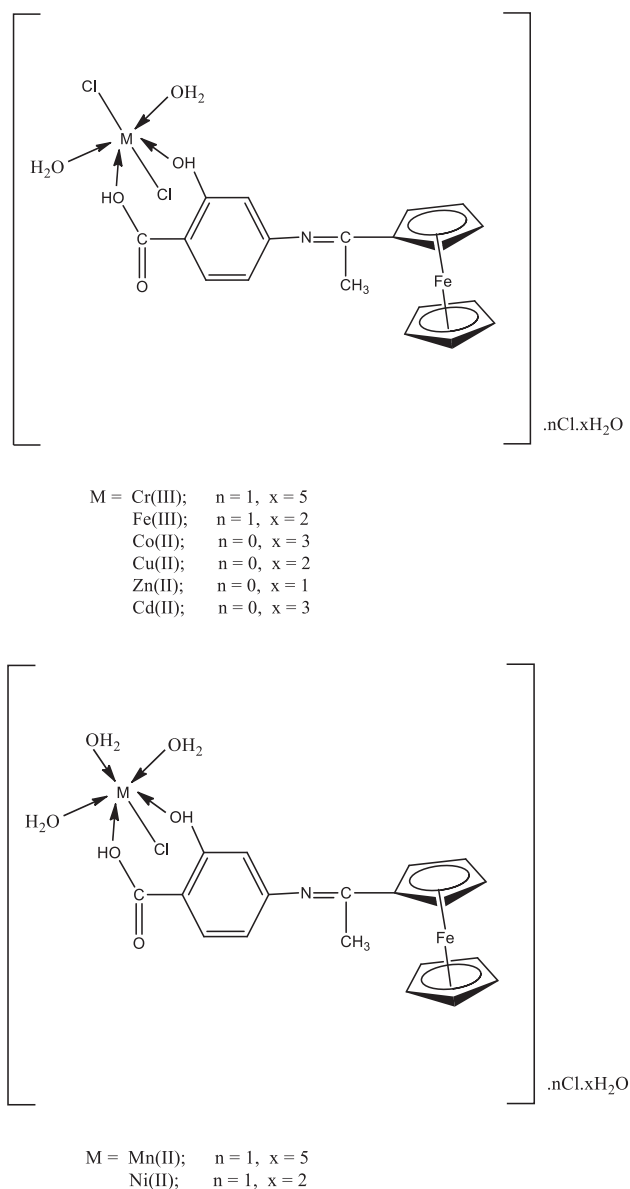


Fig. 6 The structure of organometallic Schiff base metal complexes.

3.2.7. Structural interpretation

The structure of transition metal complexes were characterized and confirmed by different spectroscopic techniques.

Also, TG and DTG thermal studies were investigated. Finally, the structure of all prepared metal complexes was shown in Fig. 6.

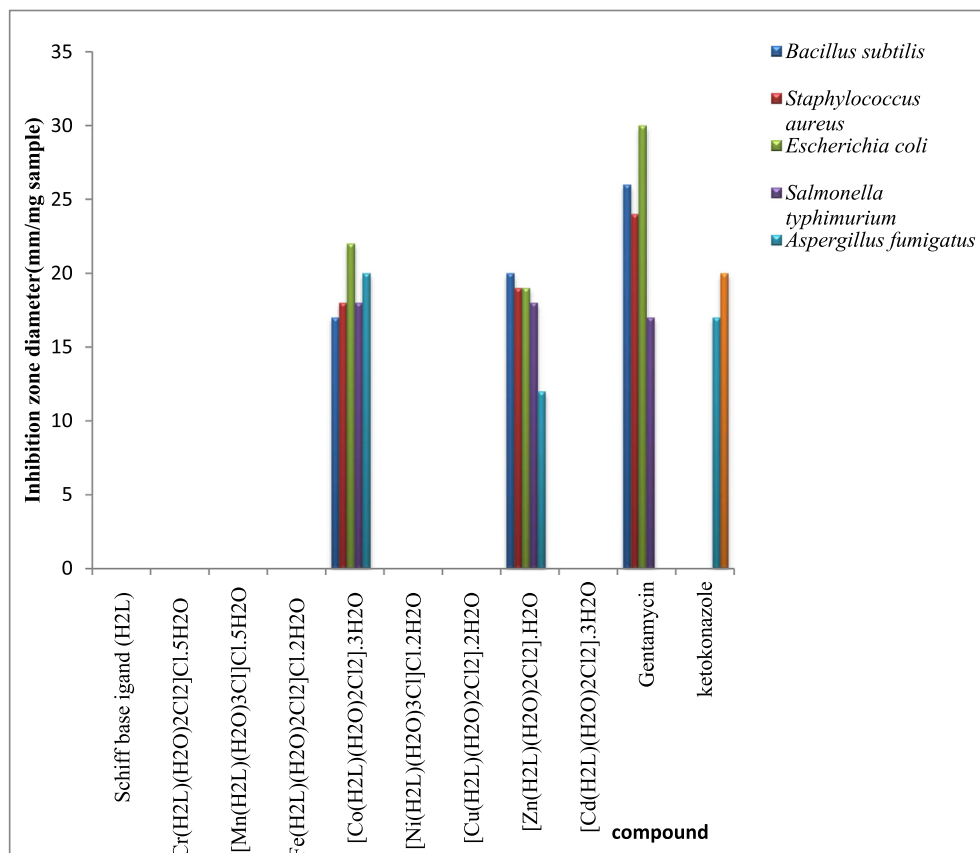


Fig. 7 Biological activity of organometallic Schiff base ligand (H₂L) and its metal complexes.

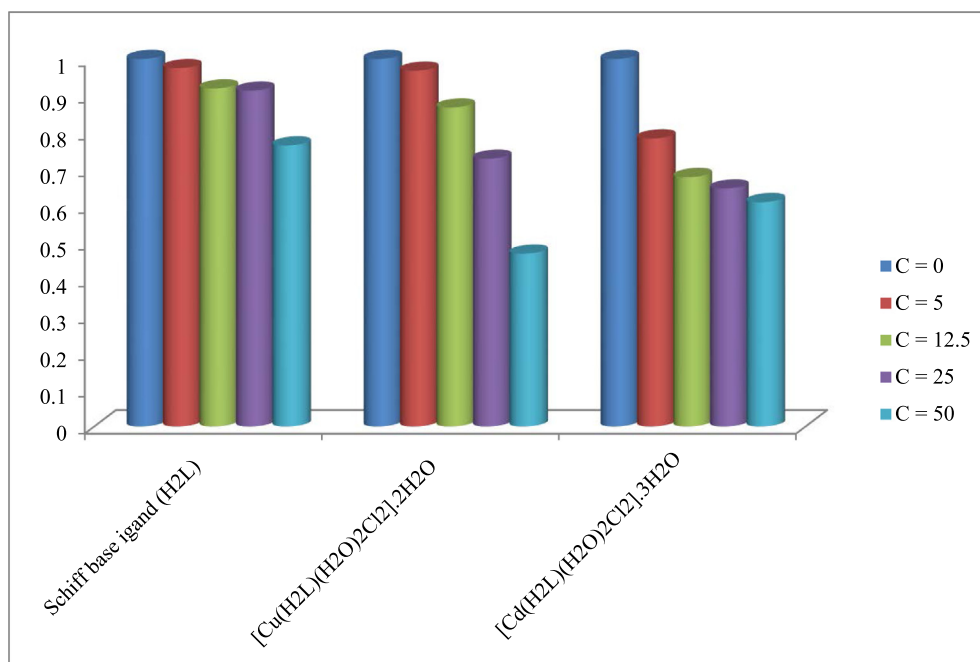


Fig. 8 Anticancer activity against breast cancer of the Schiff bases ligand (H₂L) and its metal complexes.

3.2.8. Antimicrobial activities

The main goal of the preparation of any antimicrobial compound is to help in inhibiting the causal microbe on the patients without any side effects. So, organometallic Schiff base (H₂L) and its Cr(III), Mn(II), Fe(III), Co(II), Ni(II), Cu(II), Zn(II) and Cd(II) complexes were investigated for antibacterial and antifungal activities against two strain of Gram-positive bacteria (*Bacillus subtilis* and *Staphylococcus aureus*), two strain of Gram-negative bacteria (*Escherichia coli* and *Salmonella typhimurium*) and two pathogenic fungus

(*Aspergillus fumigatus* and *Candida albicans*). The biological data were shown in Fig. 7.

The data of the biological activities of the Schiff base ligand and its metal complexes against four different bacterial and two fungal species showed that the ligand and Cr(III), Mn(II), Fe(III), Ni(II), Cu(II) and Cd(II) complexes had no activity against all species. While Co(II) and Zn(II) complexes had very high bacterial activity against all bacterial species. And also, they had fungicidal activity against *Aspergillus fumigatus* specie with inhibition zone diameter 20 and 12 mm for Co(II) and Zn(II) complexes, respectively.

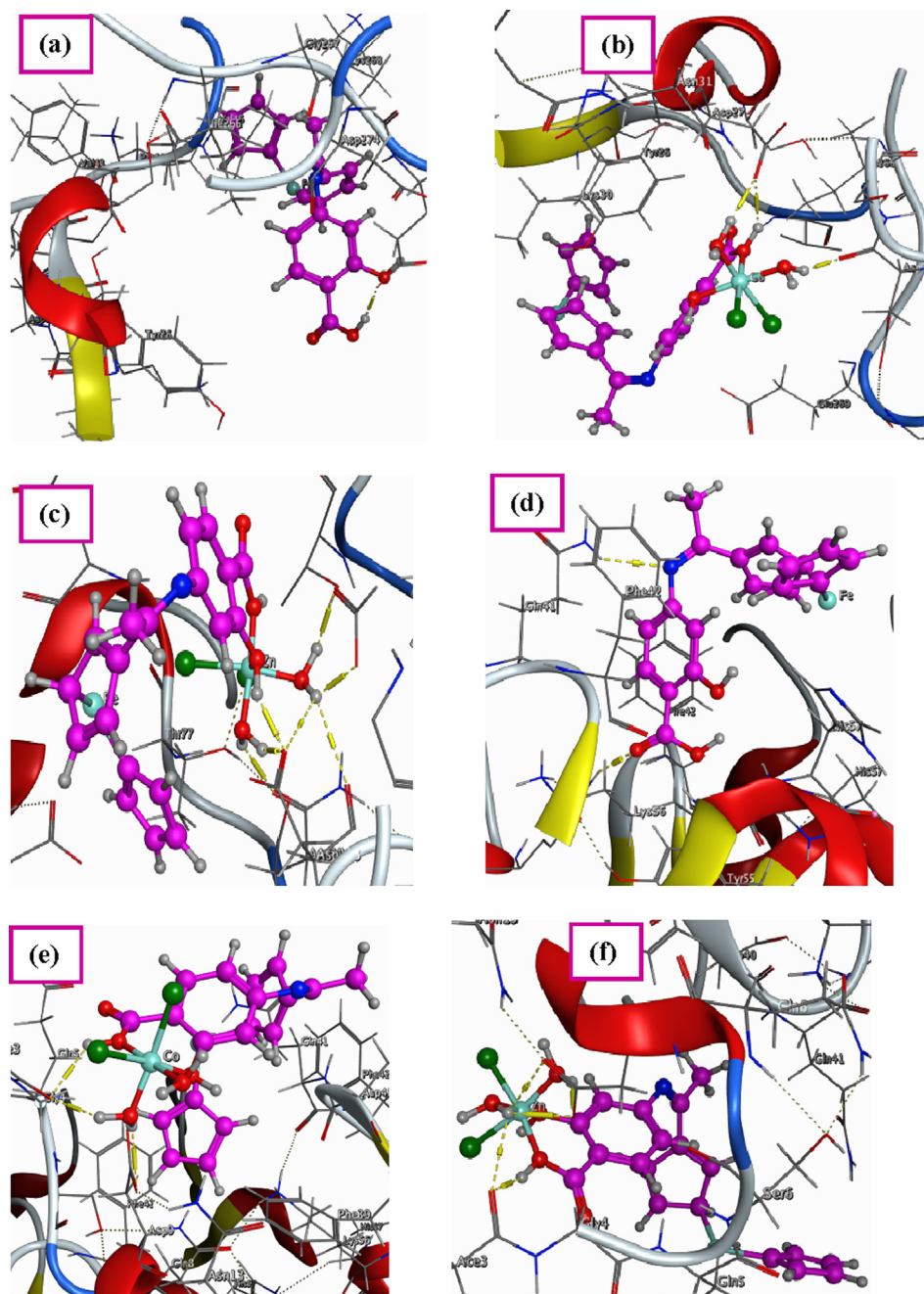


Fig. 9 3D structure of the interaction between Schiff base ligand (H₂L) with receptors of (a) 4K3V, (d) 2YLB and (g) 3DJJ, 3D plot of the interaction between Co(II) complex with receptors of (b) 4K3V, (e) 2YLB and (h) 3DJJ and 3D plot of the interaction between Zn(II) complex with receptors of (c) 4K3V, (f) 2YLB and (i) 3DJJ.

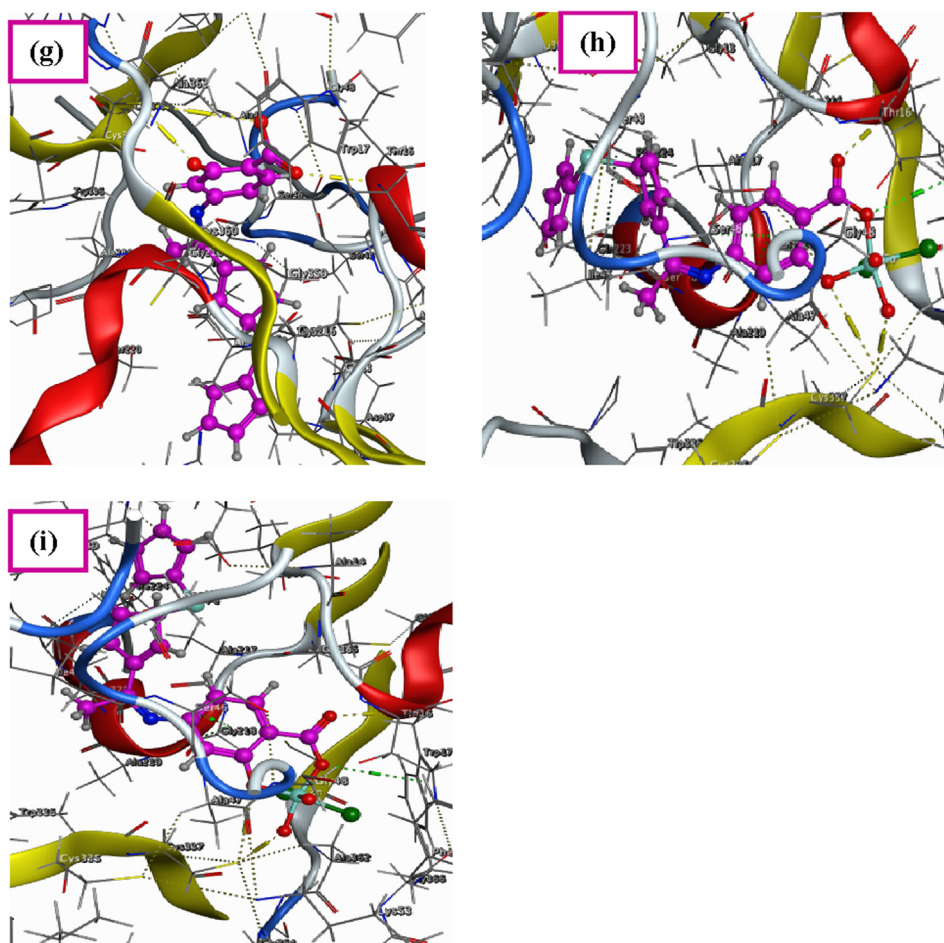


Fig. 9 (continued)

Also the activities of these compounds against Gram-positive and Gram-negative bacteria were confirmed by calculating the activity index according to the following relation (Thangadurai and Natarajan, 2001; Mahmoud et al., 2017e; Chohan et al., 2004).

$$\text{Activity index(A)} = \frac{[\text{Inhibition Zone of compound(mm)}]}{[\text{Inhibition Zone of standard drug(mm)}]} \times 100$$

From the data, it was observed that the ligand and all complexes had no activity index against all species except Co(II) and Zn(II) had very high activity index value (Mahmoud et al., 2017e).

The higher value of biological activities of some metal complexes may be attributed to their high penetrating ability to the bacteria and fungi cell wall (El-Gammal, 2010; Karekal and Mruthyunjayaswamy, 2013).

3.2.9. Anticancer activities

The in vitro cytotoxic activities of the prepared organometallic Schiff base and its metal complexes were screened against cell line of breast cancer (MCF-7). Firstly, cytotoxic activities of these compounds were calculated at single concentration 100 µg/mL against MCF-7 cell line. It was found that H₂L ligand, Cu(II) and Cd(II) complexes had inhibition ratio value 70, 74 and 78%, respectively, while other metal complexes

were < 60%. Secondary, the compounds with inhibition ratio value equal or higher than 70% were investigated against four concentrations (0, 12.5, 25 and 50 µg/mL) and the median inhibitory concentration (IC₅₀) values of these compounds were calculated. These activities were then showed in Fig. 8. From these results, it was showed that the Cu(II) complex had the lowest IC₅₀ value = 47.3 µg/mL which can be considered as very active compound that may be used in future as very effective anticancer drug (Mohamed et al., 2015).

3.2.10. Molecular modeling of organometallic Schiff base ligand (H₂L), Co(II) and Zn(II) complexes: Docking study

Docking studies is considered as very active method that can be used to establish the multi-receptor interaction of the prepared Schiff base ligand to design drug resistance against different effects that occur in our bodies (Chacko and Samanta, 2017; Rauf and Shah, 2017). So, the optimized structure of the Schiff base ligand, Co(II) and Zn(II) complexes were docked with different possible biological targets such as: the receptors of crystal structure of *Staphylococcus aureus* (PDB ID: 4K3V), crystal structure of *Salmonella typhimurium* (PDB ID: 2YLB) and crystal structure of deglycating enzyme fructosamine oxidase from *Aspergillus fumigatus* (PDB ID: 3DJJ). These bacterial and fungal species may cause some infections in skin and bone. Also, cause inflammation of

Table 5 Energy values obtained in docking calculations of Schiff base ligand (H₂L), its Co(II) and Zn(II) complexes with receptors of crystal structure of *Staphylococcus aureus* (PDB ID: 4K3V), crystal structure of *Salmonella typhimurium* (PDB ID: 2YLB) and crystal structure of deglycating enzyme fructosamine oxidase from *Aspergillus fumigatus* (PDB ID: 3DJD).

Compound	Receptor	Ligand moiety	Receptor site	Interaction	Distance (Å°)	E (kcal mol ⁻¹)	
Ligand (H ₂ L)	4K3V	O37	OE2 GLU 269	H-donor	3.00	-6.50	
		2YLB	N26	NE2 GLN 41	H-acceptor	3.22	-1.50
	3DJD	O37	NE2 GLN 8	H-acceptor	3.02	-2.00	
		O38	SG CYS 337	H-donor	3.11	-6.10	
		O37	N TRP 17	H-acceptor	2.94	-2.40	
		O37	SG CYS 337	H-donor	3.11	-4.80	
[Co(H ₂ L)(H ₂ O) ₂ Cl ₂].3H ₂ O complex	4K3V	O43	OD1 ASP 27	H-donor	2.82	-29.70	
		O46	O ASP 274	H-donor	2.85	-11.50	
		O35	OD1 ASP 27	ionic	3.11	-3.80	
		O43	OD1 ASP 27	ionic	2.82	-5.80	
		O46	OD1 ASP 27	ionic	3.31	-2.70	
		O46	OD1 ASP 27	ionic	3.31	-2.70	
	2YLB	O35	O ACE 3	H-donor	2.82	-2.80	
		O46	O ACE 3	H-donor	2.87	-3.30	
		O46	OD1 ASP 9	H-donor	2.86	-4.80	
		O46	OD2 ASP 9	H-donor	2.86	-23.00	
		O35	OD2 ASP 9	ionic	3.30	-2.80	
		O37	OD2 ASP 9	ionic	3.26	-2.90	
		O46	OD1 ASP 9	ionic	2.86	-5.50	
		O46	OD2 ASP 9	ionic	2.86	-5.50	
		3DJD	O37	SG CYS 337	H-donor	4.09	-17.50
			O43	SG CYS 337	H-donor	2.97	-43.00
			O36	N TRP 17	H-acceptor	2.82	-2.70
			C4	NH1 ARG 186	ionic	3.33	-2.60
	O43		SG CYS 337	ionic	2.97	-4.70	
	O35		5-ring TRP 17	cation-π	4.29	-2.00	
	[Zn(H ₂ L)(H ₂ O) ₂ Cl ₂].H ₂ O complex	4K3V	O37	OD1 ASP 118	H-donor	2.59	-25.50
			O42	OD1 ASN 74	H-donor	2.92	-9.50
			O42	OD1 ASP 118	H-donor	2.84	-9.50
			O45	OE1 GLU 113	H-donor	2.73	-11.30
O45			OE2 GLU 113	H-donor	2.60	-12.80	
O45			O ASP 118	H-donor	3.28	-2.00	
O45			OD1 ASP 118	H-donor	3.40	-1.30	
O35			OE1 GLU 113	ionic	2.79	-6.10	
O37			OE1 GLU 113	ionic	3.16	-3.50	
O37			OE2 GLU 113	ionic	3.04	-4.20	
O37			OD1 ASP 118	ionic	2.59	-7.90	
O42			OD1 ASP 118	ionic	2.84	-5.60	
O45			OE1 GLU 113	ionic	2.73	-6.60	
O45			OE2 GLU 113	ionic	2.60	-7.80	
O45			OD1 ASP 118	ionic	3.40	-2.30	
2YLB			O35	O ACE 3	H-donor	3.16	-2.80
			O42	OD2 ASP 9	H-donor	2.66	-10.00
			O45	O ACE 3	H-donor	3.09	-0.80
		O45	OD1 ASP 9	H-donor	3.27	-1.10	
		O45	OD2 ASP 9	H-donor	2.82	-14.50	
		O35	OD2 ASP 9	ionic	2.77	-6.20	
		O42	OD1 ASP 9	ionic	3.61	-1.50	
		O42	OD2 ASP 9	ionic	2.66	-7.20	
		O45	OD1 ASP 9	ionic	3.27	-2.90	
		O45	OD2 ASP 9	ionic	2.82	-5.80	
		3DJD	O37	SG CYS 337	H-donor	4.19	-14.10
			O42	SG CYS 337	H-donor	2.99	-42.00
O36			N TRP 17	H-acceptor	2.78	-2.50	
O42			SG CYS 337	ionic	2.99	-4.50	
O35			5-ring TRP 17	cation-π	4.30	-2.20	
6-ring	CA SER 46		π-H	4.50	-0.70		

sinuses and lungs. Three-dimensional structures of docking studies of all compounds were shown in Fig. 9. Furthermore, their binding energies with the three receptors were calculated and then were listed in Table 5.

Firstly, the ligand and its Co(II) and Zn(II) complexes were studied against receptor of Gram positive bacteria such as *Staphylococcus aureus* (PDB ID: 4K3V) (Gribenko et al., 2013). The result showed that there was possible interaction (H-donor) between the ligand and this receptor. This interaction was increased in the Co(II) and Zn(II) complexes as H-donor and ionic bonds. The minimum binding energies for ligand, Co(II) and Zn(II) complexes were -6.5 , -29.7 and -25.5 kcal mol⁻¹, respectively.

Secondary, these compounds were also investigated by molecular docking against Gram negative bacteria such as *Salmonella typhimurium* (PDB ID: 2YLB) (Sauer and Weichenrieder, 2011). The results indicated that the two complexes had stronger binding interaction with the receptor than the prepared ligand. The main interaction force of the ligand was H-acceptor while for complexes were H-donor and ionic bonds. The minimum binding energies for ligand, Co(II) and Zn(II) complexes were -2.0 , -23.0 and -14.5 kcal mol⁻¹, respectively.

Finally, the three compounds were studied against receptor of deglycating enzyme fructosamine oxidase from *Aspergillus fumigatus* (PDB ID: 3DJJ) (Collard et al., 2008). From the results, it was indicated that the main interaction force of the ligand was H-donor and H-acceptor, while in complexes some binding interaction also appeared beside the main interaction in the ligand such as ionic, cation- π and π -H. The minimum binding energies for ligand, Co(II) and Zn(II) complexes against this receptor were -6.1 , -43.0 and -42.0 kcal mol⁻¹, respectively. So, Co(II) complex showed the best binding bonds and the lowest binding energies with the different receptors. From all of this data it was confirmed that the coordination with transition metal ions increase the activities against different bacteria and fungi and so decrease the binding energy.

4. Conclusion

Eight transition metal complexes were prepared from O,O-bidentate Schiff base ligand. This ligand was synthesized by condensation of 4-aminosalicylic acid with 2-acetylferrocene. The DFT studies of the Schiff base ligand confirmed its preparation successfully by comparing the data of experimental IR and UV-Vis data with theoretical ones. All compounds then were characterized by different physicochemical and spectroscopic techniques. The data of elemental analysis confirmed that the H₂L ligand reacted with metal ions in 1:1 M ratio. IR spectra showed that ligand acted as bidentate ligand and it bound to metal ions through protonated phenolic and carboxylic groups. They had octahedral structures and they were nonelectrolyte except Cr(III), Mn(II), Fe(III) and Ni(II) complexes which were 1:1 electrolytes. After investigating, the ligand and its metal complexes against breast cancer cell line (MCF-7), it was indicated that the [Cu(H₂L)(H₂O)₂Cl₂].2H₂O complex had the lowest IC₅₀ value (47.3 μ g/mL). All compounds were screened against different bacterial species such as *Bacillus subtilis*, *Staphylococcus aureus*, *Escherichia coli* and *Salmonella typhimurium* and against two fungal species

[*Aspergillus fumigatus* and *Candida albicans*]. From these data, it was showed that Co(II) and Zn(II) complexes were only biologically active. Molecular docking studies of the free H₂L ligand and its Co(II) and Zn(II) complexes with different receptors of 4K3V, 2YLB and 3DJJ showed that the lowest binding energy were -6.5 , -2.0 and -6.1 kcal mol⁻¹ for ligand, -29.7 , -23.0 and -43.0 kcal mol⁻¹ for Co(II) complex and -25.5 , -14.5 and -42.0 kcal mol⁻¹ for Zn(II) complex, respectively. These values indicated that binding energy decreased upon coordination.

Appendix A. Supplementary material

Supplementary data to this article can be found online at <https://doi.org/10.1016/j.arabjc.2020.03.017>.

References

- Ajlouni, A.M., Abu-Salem, Q., Taha, Z.A., Hijazi, A.K. Al, Momani, W., 2016. *J. Rare Earths* 34 (10), 986.
- Aktan, E., Babur, B., Seferoglu, Z., Hokelek, T., Sahin, E., 2011. *J. Mol. Str.* 1002, 113.
- Alaghaz, A.M.A., Zayed, M.E., Alharbi, S.A., 2014a. *J. Mol. Str.* 1072 (1), 103.
- Alaghaz, A.M.A., Zayed, M.E., Alharbi, S.A., 2014b. *J. Mol. Str.* 1084, 36.
- Albert, A., 1979. *Selective Toxicity: Physico-chemical Basis of Therapy*. Wiley, New York.
- Alberto, R., 2010. *Med. Organomet. Chem.* 32, 219.
- Alothman, A.A., Al-Farraj, E.S., Al-Onazi, W.A., Almarhoon, Z.M., Al-Mohaimed, A.M., 2019. *Arabian J. Chem.* In Press.
- Alturk, S., Avci, D., Tamer, O., Atalay, Y., Sahin, O., 2016. *J. Phys. Chem. Solid* 98, 71.
- Auzias, M., Gueniat, J., Therrien, B., Suss-Fink, G., Renfrew, A.K., Dyson, P.J., 2009. *J. Organomet. Chem.* 694, 855.
- Babur, B., Seferoglu, N., Aktan, E., Hokelek, T., Sahin, E., Seferoglu, Z., 2015. *J. Mol. Str.* 1081, 175.
- Bal, M., Ceyhan, G., Avar, B., Kose, M., Kayraldiz, A., Kurtoglu, M., 2014. *Turk. J. Chem.* 38, 222.
- Balakrishnan, C., Subha, L., Neelakantan, M.A., Mariappan, S.S., 2015. *Spectrochim. Acta A* 150, 671.
- Bartholoma, M., Valliant, J., Maresca, K.P., Babich, J., Zubieta, J., 2009. *J. Chem. Commun.* 5, 493.
- Bilge, S., Kilic, Z., Hayvali, Z., Hokelek, T., Safran, S., 2009. *J. Chem. Sci.* 121 (6), 989.
- Bruijninx, P.C.A., Sadler, P., 2008. *J. Curr. Opin. Chem. Biol.* 12 (2), 197.
- Chacko, S., Samanta, S., 2017. *J. Biomed. & Pharma.* 89, 162.
- Chandra, S., Jain, D., Sharma, A.K., Sharma, P., 2009. *Molecules* 14 (1), 174.
- Chattaraj, P.K., Giri, S., 2007. *J. Phys. Chem. A* 111, 11116.
- Chohan, Z.H., Pervez, H., Rauf, A., Khan, K.M., Supuran, C.T., 2004. *J. Enzyme Inhib. Med. Chem.* 19 (5), 417.
- Collard, F., Zhang, J., Nemet, I., Qanungo, K.R., Monnier, V.M., Yee, V.C., 2008. *J. Biol. Chem.* 283 (40), 27007.
- Dennington, R., Keith, T., Millam, J., editors. 2009. *GaussView, Version 5.0.8*, R. KS: Dennington, Semicem Inc., Shawnee Mission.
- Dhanaraj, C.J., Hassan, I.U., Johnson, J., Joseph, J., Joseyphus, R.S., 2016. *J. Photochem. & Photobio. B* 162, 115.
- Ekmekcioglu, P., Karabocek, N., Karabocek, S., Emirik, M., 2015. *J. Mol. Str.* 1099, 189.
- El-Gammal, O.A., 2010. *Spectrochim. Acta A* 75, 533.
- Ermis, E., 2018. *J. Mol. Str.* 1156, 91.

- Firouzabadi, A.A.D., Firouzmandi, S., 2017. *J. Braz. Chem. Soc.* 28 (5), 768.
- Fouda, M.F.R., Abd-Elzaher, M.M., Abdelsamaia, R.A., Labib, A. A., 2007. *Appl. Organomet. Chem.* 21 (8), 613.
- Frisch, M.J., et al., 2004. Gaussian 03, Revision C.01, Gaussian Inc, Wallingford CT.
- Gaber, M., El-Ghamry, H.A., Fathalla, Sh.K., Mansour, M.A., 2018. *Mater. Sci. & Eng. C* 83, 78.
- Geerlings, P., Proft, F.D., Langenaeker, W., 2003. *Chem. Rev.* 103 (5), 1793.
- Gokce, H., Ozturk, N., Kazici, M., Goreci, C.Y., Günes, S., 2017. *J. Mol. Str.* 1136, 288.
- Govindaraj, V., Ramanathan, S., 2014. *Turk. J. Chem.* 38, 521.
- Gribenko, A., Mosyak, L., Ghosh, S., Parris, K., Svenson, K., Moran, J., Chu, L., Li, S., Liu, T., Woods, V.L., Jansen, K.U., Green, B.A., Anderson, A.S., Matsuka, Y.V., 2013. *J. Mol. Biol.* 425, 3429.
- Gull, P., Hashmi, A.A., 2015. *J. Braz. Chem. Soc.* 26 (7), 1331.
- Halli, M.B., Patil, V.B., Bevinamarada, S.R., 2011. *Turk. J. Chem.* 35, 393.
- Hillard, E.A., Vessieres, A., Bideau, F.L., Plazuk, D., Spera, D., Huche, M., Jaouen, G., 2006. *Chem. Med. Chem.* 1, 551.
- Karekal, M.R., Mruthyunjayaswamy, B.H.M., 2013. *Turk. J. Chem.* 37, 775.
- Kealy, T.J., Pauson, P.L., 1951. *Nature* 168 (4285), 1039.
- Kianfar, A.H., Ramazani, S., Fath, R.H., Roushani, M., 2013. *Spectrochim. Acta A* 105, 374.
- Kopf-Maier, P., Kopf, H., Neuse, E.W., 1984. *J. Cancer Res. Clin.* 108 (3), 336.
- Kucuk, H.B., Kara, E.M., Celik, B.O., 2015. *Turk. J. Chem.* 39, 939.
- Lakshmipraba, J., Arunachalam, S., Solomon, R.V., Venuvanalingam, P., 2015. *J. Coord. Chem.* 68 (8), 1374.
- Liu, H., Wang, H., Gao, F., Niu, D., Lu, Z., 2007. *J. Coord. Chem.* 60 (24), 2671.
- Mahalakshmi, N., Rajavel, R., 2010. *Arabian J. Chem.* In Press.
- Mahmoud, W.H., Deghadi, R.G., Mohamed, G.G., 2017a. *J. Therm. Anal. Calorim.* 127 (3), 2149.
- Mahmoud, W.H., Mahmoud, N.F., Mohamed, G.G., 2017b. *Appl. Organomet. Chem.* 31 (12), e3858.
- Mahmoud, W.H., Mahmoud, N.F., Mohamed, G.G., 2017c. *J. Coord. Chem.* 70 (20), 3552.
- Mahmoud, W.H., Mohamed, G.G., Refat, A.M., 2017d. *Appl. Organomet. Chem.* 31 (11), e3753.
- Mahmoud, W.H., Mohamed, G.G., El-Sayed, O.Y., 2017e. *Appl. Organomet. Chem.* 32 (2), e4051.
- Mahmoud, W.H., Omar, M.M., Sayed, F.N., 2016. *J. Therm. Anal. & Calorim.* 124 (2), 1071.
- Martins, D.A., Filho, L.F.B., da Silva, C.M., de Fátima, A., Louro, S. R.W., Batista, D.G.L., Soeiro, M.N.C., de Carvalhod, J.E., Teixeira, L.R., 2017. *J. Braz. Chem. Soc.* 28 (1), 87.
- Mohamed, G.G., Abd El-Wahab, Z.H., 2005. *Spectrochim. Acta A* 61, 1059.
- Mohamed, G.G., Omar, M.M., Hindy, A.M., 2006. *Turk. J. Chem.* 30, 361.
- Mohamed, G.G., Zayed, E.M., Hindy, A.M.M., 2015. *Spectrochim. Acta A* 145, 76.
- Mudi, S.Y., Usman, M.T., Ibrahim, S., 2015. *American J. Chem. & Appl.* 2 (6), 151.
- Rauf, A., Shah, A., 2017. *Arabian J. Chem.* In Press.
- Pearson, R.G., 1989. *J. Organomet. Chem.* 54 (6), 1423.
- Popova, L.V., Babin, V.N., Belousov, Y.A., Nekrasov, Y.S., Snegireva, A.E., Borodina, N.P., Shaposhnikova, G.M., Bychenko, O. B., Raevskii, P.M., 1993. *Appl. Organomet. Chem.* 7 (2), 85.
- Reed, A.E., Curtiuss, L.A., Weinhold, F., 1988. *Chem. Rev.* 88 (6), 899.
- Roman, G., Andree, M., 2001. *Bull. Chem. Technol. Macedonia.* 20 (2), 131.
- Sagdinc, S., Koksoy, B., Kandeirli, F., Bayari, S.H., 2009. *J. Mol. Str.* 917, 63.
- Sahin, O., Ozdemir, U.O., Seferoglu, N., Genc, Z.K., Kaya, K., Aydiner, B., Tekin, S., Seferoglu, Z., 2017. *J. Photochem. & Photobio. B* 178, 428.
- Samouei, H., Rashidi, M., Heinemann, F.W., 2011. *J. Organomet. Chem.* 696, 3764.
- Sauer, E., Weichenrieder, O., 2011. *Proc. Natl. Acad. Sci. USA* 108 (32), 13065.
- Scheck, R.A., Schepartz, A., 2011. *Acc. Chem. Res.* 44 (9), 654.
- Singh, B.K., Mishra, P., Prakash, A., Bhojak, N., 2012. *Arabian J. Chem.* In Press.
- Singh, K., Puri, P., Dharampal, 2010. *Turk. J. Chem.* 34, 499.
- Skehan, P., Storeng, R., Scudiero, D., Monks, A., McMahon, J., Vistica, D., Warren, J.T., Bokesch, H., Kenney, S., Boyd, M.R., 1990. *J. National Cancer Instit.* 82 (13), 1107.
- Soliman, M.H., Mohamed, G.G., 2013. *Spectrochim. Acta A* 107, 8.
- Thangadurai, T.D., Natarajan, K., 2001. *Indian J. Chem. A* 40 (6), 573.
- Yadav, S., Singh, R.V., 2011. *Spectrochim. Acta A* 78, 298.
- Zhang, Y.H., Yuan, J.C., Lao, W.J., Yin, Y.Q., Huang, Z.X., Wu, J.J., 2001. *J. Organomet. Chem.* 628, 123.